Toughening mechanisms in nacre-like alumina revealed by in-situ imaging of stress

Hassan Saad, Thierry Douillard, Annie Malchère, Philippe Steyer, Sylvain Meille, Sylvain Deville, Bruno Reynard

Toughening mechanisms in nacre-like alumina revealed by in-situ imaging of stress

Hassan Saad[1, 2], Thierry Douillard[2], Annie Malchère[2],
Philippe Steyer[2], Sylvain Meille[2], Sylvain Deville[1, 3],
and Bruno Reynard[4,*]

[1] *Laboratoire de Synthèse & Fonctionnalisation des Céramiques,*
UMR3080 CNRS-Saint-Gobain CREE,
Saint-Gobain Research Provence, 84306 Cavaillon, France

[2] *Univ Lyon, INSA Lyon, MATEIS CNRS UMR5510, Villeurbanne, France*

[3] *Université de Lyon, Université Claude Bernard Lyon 1, CNRS,*
Institut Lumière Matière, 69622 Villeurbanne, France

[4] *Univ Lyon, ENS-Lyon, CNRS, LGL-TPE, UMR 5276,*
46 allée d'Italie, F-69364 Lyon cedex 07, France

(Dated: June 14, 2022)

* corresponding author: bruno.reynard@ens-lyon.fr

Abstract. Nacre-like aluminas are bio-inspired, ceramic-based composites that display high toughness and strength. Their toughness arises from their brick-and-mortar microstructure. We must understand the role of several microstructural features over their mechanical properties. Techniques that allow microstructural imaging during mechanical tests are therefore desired. Here, we use both *in situ* fluorescence spectroscopy to image the stress field around cracks propagating in samples, and *in situ* scanning electron microscopy to image the crack-microstructure interactions. Stress concentrates around locally disordered zones where the crack is pinned while crack propagation is delayed. *In situ* imaging shows that obstacles to crack propagation are either larger-than-average alumina platelets or bundles of alumina platelets misaligned with respect to the majority of the platelets. Such microstructural heterogeneities are therefore important to impede crack propagation in nacre-like alumina. The approach proposed here can be used to understand the structure/properties relationships of other types of materials.

Keywords: *mechanical behavior, toughness, scanning electron microscopy, fluorescence spectroscopy, ceramic composites*

Graphical abstract

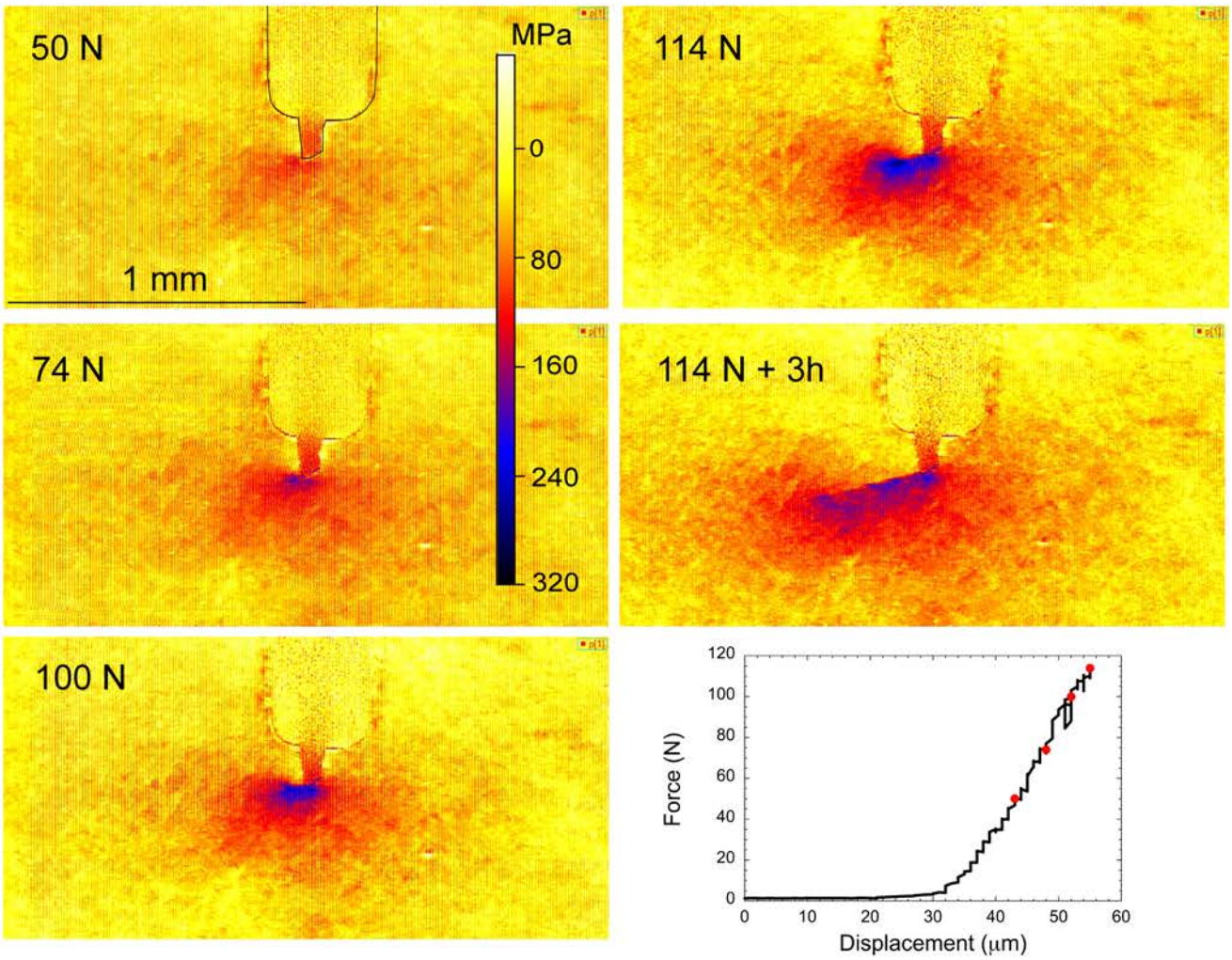

Images of stress and crack propagation in single-edge notched beam of nacre-like alumina submitted to increasing force

1. Introduction

Strength and toughness are mutually exclusive properties of materials in general and ceramics in particular. Designs found in biological structural materials such as nacre may provide useful guidelines to alleviate this trade-off (Ritchie, 2011). Nacre-like alumina, made of brittle constituents only, combines the hardness and strength of standard alumina materials, and comparatively high toughness. This toughness (damage resistance) is achieved mostly by the deviation of cracks along the platelets interface in their brick-and-mortar microstructure (Bouville et al., 2014). While the deviation of cracks in brick-and-mortar microstructures is well documented, several other toughening mechanisms can exist in biological or bio-inspired materials (Bouville, 2020; Kakisawa and Sumitomo, 2011). Discrete elements modeling (DEM) has been implemented to understand the toughening mechanisms of nacre-like alumina and provide guidelines of microstructural features to implement to improve the damage resistance of these composites (Radi et al., 2020). Establishing quantitative links between nano- to microscopic structures and bulk mechanical properties determined in standardized fracture tests requires additional mechanical modeling at various scales and methods that enable imaging the effects of microstructures on the mechanical behavior. For instance, structural defects (such as local misalignments, variable platelet size) of real microstructures spanning few tens of micrometers can be modeled by DEM, which suggests that they may have a significant effect on crack propagation (Radi et al., 2021). To validate these results, we developed *in situ* spectroscopic and scanning electron microscopy (SEM) imaging of stress field and microstructure during a bending test on nacre-like alumina.

2. Materials and methods

Samples were prepared as standard single-edge notched beams (SENB), and mirror polished before testing (Saad et al., 2020). 3 × 6 × 36 mm samples were used for fluorescence spectroscopy and SEM characterization. The fluorescence of trivalent chromium (Cr^{3+}), a ubiquitous impurity in

alumina-based polycrystalline ceramics, was used to map stresses in the composite (Pezzotti et al., 2012; Portu et al., 2005). Even in very low quantities (< 0.5 wt%), Cr^{3+} causes an intense fluorescence characterized by two sharp and intense lines, noted R_1 and R_2, whose energy shifts with applied stress (Feher and Sturge, 1968; He and Clarke, 1995).

We used a Horiba™ LabRam HRevolution Raman spectrometer equipped with a motorized stage for mapping the fluorescence signal excited with a 532-nm solid-state diode laser from SENB submitted to a four-point bending test. The laser is focused through a microscope equipped with a long-working distance x50 Mitutoyo™ objective down to a spot of about 1µm. The high fluorescence signal allows a typical recording time τ of the order of one millisecond or less to obtain an intense enough fluorescence spectrum at each point and determine peak position and stress. X-Y maps of the sample lateral surface were obtained in the SWIFT™ mode where the sample is scanned at constant speed in the X direction (perpendicular to the notch, see Figure 1 left) under the laser, and signal-processed through the CCD detector to record individual points every τ. Spatial resolution is determined by the product of the scanning speed and reading time τ in the X direction, and by step-by-step motion in the Y direction (along notch). Identical steps were chosen in both X and Y directions to avoid potential distortion in the image, and set to 5 and 2 µm for low- and high-resolution images, respectively. Low-resolution images covering a 1 × 2 mm^2 field of view and high-resolution images covering 300 x 750 μm^2 were acquired in about one minute each around the crack. One image with steps of 0.5 µm over a 400 × 150 μm^2 area was acquired in 40 minutes at the end of the test (corresponding to a long crack propagation but without macroscopic failure of the sample) for comparison with post mortem imaging by SEM. The stress was maintained at a set value at each step while maps were acquired. With the optical setting and characteristics of the laser-material interaction, the actual resolution is better than 2 µm.

The R_1 position shifts by $\Delta\nu$ with the applied stress σ as:

$$\Delta\nu = \Pi\sigma \quad (1).$$

$\Pi = 1/3\ \partial\nu/\partial P = 2.5\ \mathrm{cm^{-1}.GPa^{-1}}$ is the average piezospectroscopic coefficient with P the hydrostatic pressure, $\Pi_c = 1.5\ \mathrm{cm^{-1}.GPa^{-1}}$ is the piezospectroscopic coefficient along the c direction and $\Pi_a = 3.0\ \mathrm{cm^{-1}.GPa^{-1}}$ is the average piezospectroscopic coefficient perpendicular to the c direction of corundum lattice (Feher and Sturge, 1968; He and Clarke, 1995). In the nacre-like microstructure the macroscopic applied tensile stress is parallel to the basal plane of most alumina platelets (or corundum structure), but the local stress field near the notch is not uniaxial. The average value of $2.5\ \mathrm{cm^{-1}.GPa^{-1}}$ for the piezospectroscopic coefficient was used here, which is sufficient for imaging and following the spatial and temporal changes in stress. Stress fluctuations in homogeneous areas yield an estimated uncertainty on relative values of stress of 40 MPa from pixel to pixel, and less than 15 MPa for 3 × 3 pixel squares, *i.e.* over about 15 microns for low resolution images, and 6 or 3 microns for higher resolution images.

The sample tested *in situ* with fluorescence spectroscopy was characterized post operando with a SUPRA 55VP SEM. Due to the elastic spring back, the crack was not open anymore and its exact trajectory in the complex microstructure was determined by comparison with the high-resolution fluorescence image. A complementary SEM *in situ* analysis was performed on another SENB sample. The SUPRA SEM allows working at low acceleration voltage without metallization of the surface, which preserves the microstructure. In these conditions, back-scattered electrons are subjected to electron channeling that enhances the contrast between phases, highlighting the nacre-like microstructure (Lafond et al., 2021).

3. Results

Starting from an initial state with negligible stress, the evolution of the stress map calculated from large fluorescence maps (Fig. 1) shows, the tensile stress field that develops around the crack tip

as applied force increases (Fig. 1). Tensile stresses are detected while the sample is still in the elastic domain, and well before the crack initiation. The stress field is asymmetric with the side at higher stress (left of the notch in Figure 1) eventually fracturing with a crack initiating at about 70° of the notch plane for an applied force of 110 N. Before the crack can be observed at the surface of the sample, the area under tension remains constant and does not increase in size, only the value of the calculated stress increases with the loading force to exceed locally 300 MPa. While the crack extends, the tip of the uncracked ligament is subjected to important tensile stresses, with average values up to 250 MPa. The tensile nature of the stress field generated at the bottom of the notch is coherent with the SENB configuration

At an applied force of 110 N, the first high-resolution image recorded (Fig. 2) shows a stress accumulation pinned on a mechanical asperity along the crack (point 1). The force was increased to 114 N, and the sample was then maintained at a constant force for several hours. High-resolution maps display the evolution of the stress field, which highlight mechanical asperity effects during sub-critical crack propagation. The crack first propagated towards a second mechanical asperity (point 2) after the first low-resolution map was recorded at 114 N (about 10 minutes), and did not evolve with the force maintained at 114 N for at least 1.5 hours. The stress concentration zone then transferred to point 3 after 3 hours (Fig. 1), due to progressive cracking of mechanical bridges that hindered crack propagation at point 2. The microstructure did not evolve when the last map was recorded after 4 hours at 114 N (Fig. 2). The separation between each mechanical asperity is roughly 100 μm, from defect 0 (notch tip) to defect 3.

Progressively, the stress transfer along the crack is accompanied by a decrease of the tensile stress field around the crack tip, with final values around 250 MPa. Further propagation of the crack would require building a sufficient stress field at the tip of the crack to break the asperity on which it is now pinned. The sub-critical propagation is promoted by the initial high tensile stress surrounding the crack tip at point 1. When the loading force is maintained constant, and as long as the stress at the

crack tip exceeds the fracture properties of the interface, the crack propagates by jumping from one defect to the other. It took about 2 hours to jump from point 2 to point 3.

To better visualize the stress distribution around the crack tip after sub-critical crack propagation, a higher resolution fluorescence map was recorded in the area containing the crack while the load was maintained at 114 N for 40 minutes, for comparison with microstructural SEM imaging. The contrast between the area under tension and compression reveals the crack path and can be overlaid with the SEM image of the same area (Fig. 3).

The crack path up to its tip (point 3) can be located from a sharp contrast between the mechanically relaxed areas (yellowish tones) above the crack and those under tensile stress below it. A major crack is outlined by yellowish tones next to reddish ones, and secondary cracks branch on it and separate reddish areas from bluish ones. Between the notch and the crack tip, the points where crack pinning and stress accumulation was noted during the test (Fig. 2) correspond to specific defects in the microstructure as observed from the surface. At point 1, the crack had to bypass a cluster of misaligned platelets, resulting in a diverted trajectory and stress contrast that contours both sides of the cluster. At point 2, branching is observed with a secondary crack seemingly appearing below a larger-than-average alumina platelet. At point 3, the crack is again pinned on a cluster of misoriented alumina platelets, and a very local stress concentration is observed before the experiment was stopped after 4 hours at a force of 114 N.

The nature of microstructural defects involved in crack deviation and branching was further characterized using in situ SEM imaging of another SENB sample under stress. Similar behaviors and features were observed with fast crack propagation steps separated by arrests. With *in situ* imaging, the active cracks are open and can be directly visualized (Fig. 4) whereas in a posteriori characterization, cracks are closed and their exact location in the complex contrasts of the microstructure is more difficult to determine (Fig. 3). Although the sample used for *in situ* SEM was different from the one used in fluorescence mapping, similar microstructural features are associated to crack deviation and

branching.

Discussion and concluding remarks

When SENB four-point experiments are performed on non-textured ceramics, the crack initiates and propagates along the notch plane. Strong crack deviation from the notch plane here is due to the anisotropic microstructure of the material. This crack deviation is linked to the contrasted mechanical properties between alumina platelets (brick) and the aluminosilicate glass phase (mortar) (Bouville et al., 2014; Henry et al., 2020; Jackson et al., 1988; Kakisawa and Sumitomo, 2011). Optimization of brick-and-mortar materials has thus far relied on mechanical tests on bulk samples and numerical models that both assume structural homogeneity from the microscopic to the macroscopic level. This may be true for the well-ordered nacre. However, the actual structure of nacre-like ceramics is more complex, with heterogeneity in alumina platelet size and imperfect orientations during the fabrication (Saad et al., 2020). Simulations based on actual microstructures have shown the importance of local imperfections of the microstructure on the toughness of the composite (Marcinkowska, 2018; Radi et al., 2021). Imaging of local stress around the propagating crack highlights the interaction of the crack with the imperfections of the microstructure.

Fluorescence maps revealed important stress gradients near the tip of the notch, with variations of up to 300 MPa in a few micrometers. This is lower than the strength of platelets around 1 GPa (Doitrand et al., 2020; Feilden et al., 2017), but higher than the yield strength of aluminosilicate glasses used as mortar along the interfaces (Bouville et al., 2014; Saad et al., 2020), with values lower than 100 MPa (Sheikh et al., 2019). Even if a calculation of local stresses considers hydrostatic stresses and is based on the hypothesis of isotropy in piezospectroscopic coefficient (thereby not capturing the texture of this material), the stress values are coherent. These calculated stress values likely reflect the effects of the textural heterogeneities on local mechanical properties. In particular, bundles of alumina platelets oriented at high angles with respect to the main orientation of platelets in

the microstructure are likely to play a role because platelets cannot be broken along a mechanically strong direction of the platelets. Thus the crack has to deviate along an easier path, the weaker aluminosilicate interphase (Figs. 3 and 4). This is consistent with the results of numerical simulations that used the observed microstructures to show cracks propagate at higher stress around bundles of misoriented platelets, thus contributing to toughening the composite (Radi et al., 2021). These defects likely contribute to the increasing toughness (R curve) of the nacre-like alumina. High-stress gradients are clearly associated with defects, in spite of the intrinsic limitation that the observation is performed on the surface of a 3D sample.

In situ fluorescence mapping of stress and SEM imaging during mechanical tests prove useful to identify local mechanisms and microstructural features that contribute to toughening in these bioinspired composites. Future improvements will focus on measurements that can be combined on the same sample and use the orientation information provided by EBSD to locally analyze the stress from the scale of the individual components (here the alumina platelets) to the scale of the aggregate (platelets bundles) and of the bulk sample. Besides using fluorescence, stress can also be characterized using Raman spectroscopy in non-luminescent materials. This approach could be applied to other advanced ceramics like zirconia, or natural ceramics like apatite and calcium carbonates (Loh et al., 2020; Perrichon et al., 2017; Pezzotti and Sakakura, 2003; Pezzotti et al., 2012; Wei et al., 2020; Zhu and Pezzotti, 2011).

Acknowledgments

We acknowledge the technical support of Saint-Gobain Research Provence. This research was funded through project BICUIT by Agence Nationale pour la Recherche (ANR-16-CE08-0006, project BICUIT). INSU-CNRS and LABEX Lyon Institute of Origins (ANR-10-LABX-0066) support the Raman facility at ENS de Lyon.

Conflict of interest. The authors declare no conflict of interest.

212

213 **References**

214 Bouville, F., 2020. Strong and tough nacre-like aluminas: Process–structure–performance relationships
215 and position within the nacre-inspired composite landscape. Journal of Materials Research 35,
216 1076-1094.

217 Bouville, F., Maire, E., Meille, S., Van de Moortèle, B., Stevenson, A.J., et al., 2014. Strong, tough and
218 stiff bioinspired ceramics from brittle constituents. Nature Materials 13, 508-514.

219 Doitrand, A., Henry, R., Saad, H., Deville, S., Meille, S., 2020. Determination of interface fracture
220 properties by micro- and macro-scale experiments in nacre-like alumina. Journal of the
221 Mechanics and Physics of Solids 145, 104143.

222 Feher, E., Sturge, M.D., 1968. Effect of Stress on the Trigonal Splittings of d^3 Ions in Sapphire (a-
223 Al_2O_3). Physical Review 172, 244-249.

224 Feilden, E., Giovannini, T., Ni, N., Ferraro, C., Saiz, E., et al., 2017. Micromechanical strength of
225 individual Al_2O_3 platelets. Scripta Materialia 131, 55-58.

226 He, J., Clarke, D.R., 1995. Determination of the Piezospectroscopic Coefficients for Chromium-Doped
227 Sapphire. Journal of the American Ceramic Society 78, 1347-1353.

228 Henry, R., Saad, H., Doitrand, A., Deville, S., Meille, S., 2020. Interface failure in nacre-like alumina.
229 Journal of the European Ceramic Society 40, 4694-4699.

230 Jackson, A.P., Vincent, J.F.V., Turner, R.M., Alexander, R.M., 1988. The mechanical design of nacre.
231 Proceedings of the Royal Society of London. Series B. Biological Sciences 234, 415-440.

232 Kakisawa, H., Sumitomo, T., 2011. The toughening mechanism of nacre and structural materials
233 inspired by nacre. Science and Technology of Advanced Materials 12, 064710.

234 Lafond, C., Douillard, T., Saad, H., Deville, S., Meille, S., et al., 2021. eCHORD orientation mapping
235 of bio-inspired alumina down to 1 kV. Materialia 20, 101207.

236 Loh, H.-C., Divoux, T., Gludovatz, B., Gilbert, P.U.P.A., Ritchie, R.O., et al., 2020. Nacre toughening

due to cooperative plastic deformation of stacks of co-oriented aragonite platelets. Communications Materials 1, 77.

Marcinkowska, M., 2018. Elaboration and characterization of mechanical properties of ceramic composites with controlled architecture - Elaboration et caracterisation des propriétés mécaniques de composites céramiques à architecture contrôlée. Université de Lyon.

Perrichon, A., Reynard, B., Gremillard, L., Chevalier, J., Farizon, F., et al., 2017. A testing protocol combining shocks, hydrothermal ageing and friction, applied to Zirconia Toughened Alumina (ZTA) hip implants. Journal of the Mechanical Behavior of Biomedical Materials 65, 600-608.

Pezzotti, G., Sakakura, S., 2003. Study of the toughening mechanisms in bone and biomimetic hydroxyapatite materials using Raman microprobe spectroscopy. Journal of Biomedical Materials Research Part A 65A, 229-236.

Pezzotti, G., Takahashi, Y., Zhu, W., Sugano, N., 2012. In-depth profiling of elastic residual stress and the in vivo wear mechanism of self-mating alumina hip joints. Wear 284–285, 91-97.

Portu, G.d., Micele, L., Sekiguchi, Y., Pezzotti, G., 2005. Measurement of residual stress distributions in Al_2O_3/3Y-TZP multilayered composites by fluorescence and Raman microprobe piezo-spectroscopy. Acta Materialia 53, 1511-1520.

Radi, K., Jauffres, D., Deville, S., Martin, C.L., 2020. Strength and toughness trade-off optimization of nacre-like ceramic composites. Composites Part B: Engineering 183, 107699.

Radi, K., Saad, H., Jauffres, D., Meille, S., Douillard, T., et al., 2021. Effect of microstructure heterogeneity on the damage resistance of nacre-like alumina: Insights from image-based discrete simulations. Scripta Materialia 191, 210-214.

Ritchie, R.O., 2011. The conflicts between strength and toughness. Nature Materials 10, 817-822.

Saad, H., Radi, K., Douillard, T., Jauffres, D., Martin, C.L., et al., 2020. A simple approach to bulk bioinspired tough ceramics. Materialia 12, 100807.

Sheikh, M.Z., Zhen, W., Tao, S., Yulong, L., Fenghua, Z., et al., 2019. Dynamic failure of un-

strengthened aluminosilicate glass. Theoretical and Applied Fracture Mechanics 104, 102325.

Wei, C., Montagnac, G., Reynard, B., Le Roux, N., Gremillard, L., 2020. Interplay between internal stresses and matrix stiffness influences hydrothermal ageing behaviour of zirconia-toughened-alumina. Acta Materialia 185, 55-65.

Zhu, W., Pezzotti, G., 2011. Raman analysis of three-dimensionally graded stress tensor components in sapphire. Journal of Applied Physics 109, 073502.

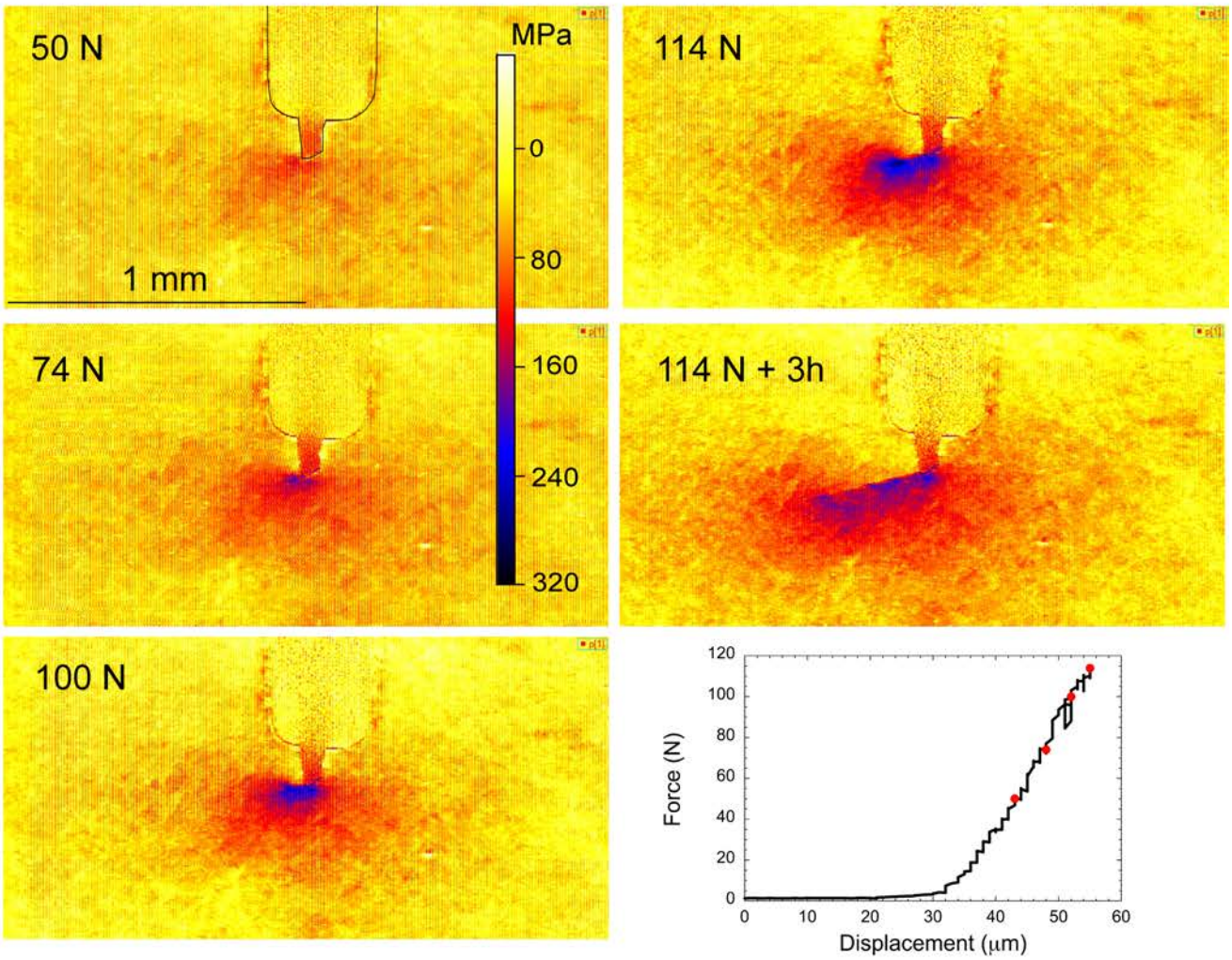

Figure 1. Evolution of the stress measured using Cr^{3+} fluorescence in SENB under increasing force (values in N) up to crack initiation and propagation at 114N. Corresponding points are indicated by the red dots on the force-displacement curves (bottom right). The stress field locates and concentrates on the left side of the notch materialized by the thin black outline on the 50N stress map. As the load increases, the stress locally reaches values of ~250 MPa. The thin black line outlines the position of the notch.

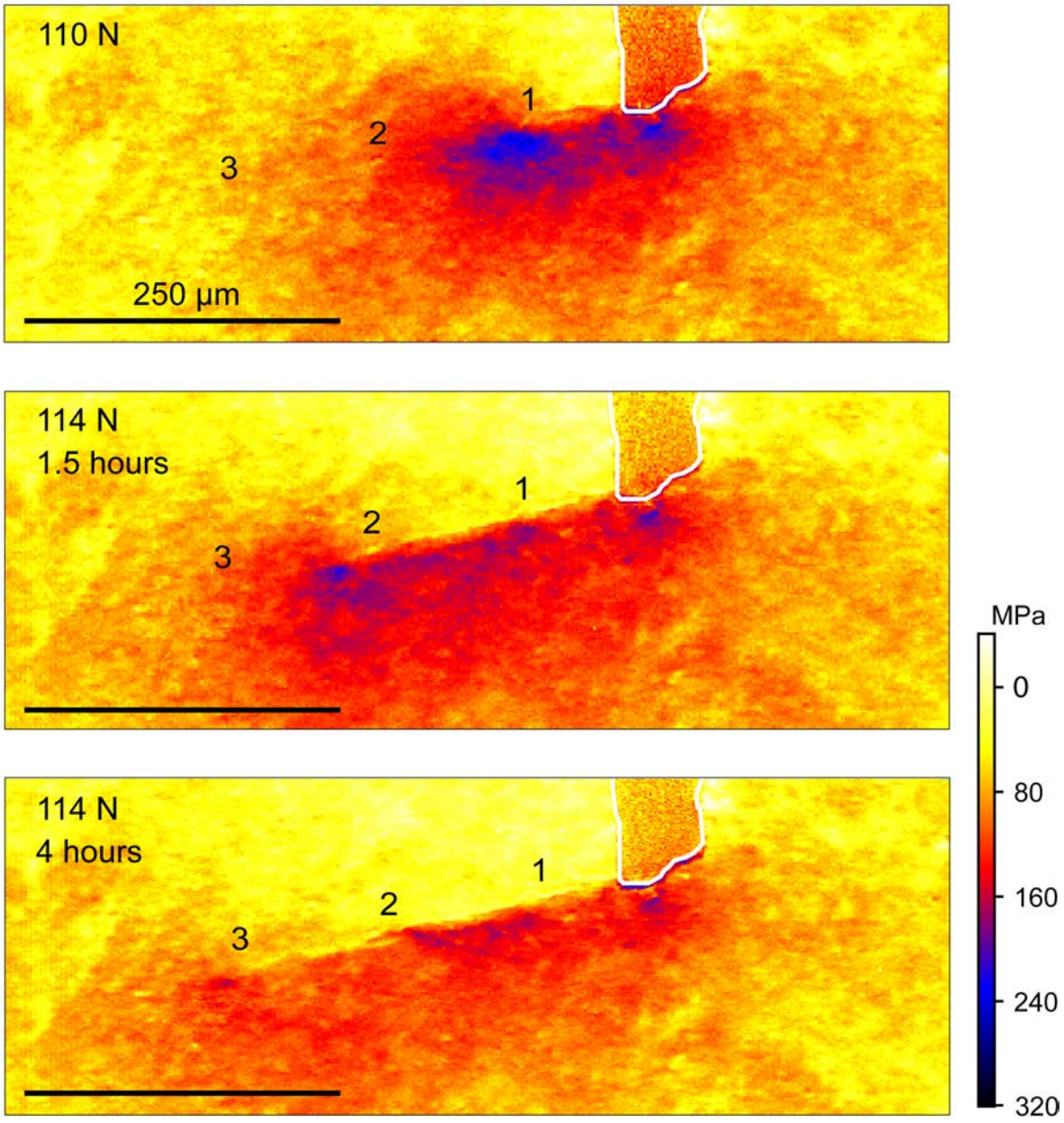

Figure 2. Sub-critical crack propagation. The high tensile stress field present at the crack tip is highlighted. Crack propagation is accompanied by a reduction of the stress intensity at the crack tip. The stress field is pinned on mechanical asperities labeled 1 to 3 that contribute to the crack propagation resistance of the material. The white line outlines the position of the notch. © (2022) H. Saad et al. (10.6084/m9.figshare.20072111)

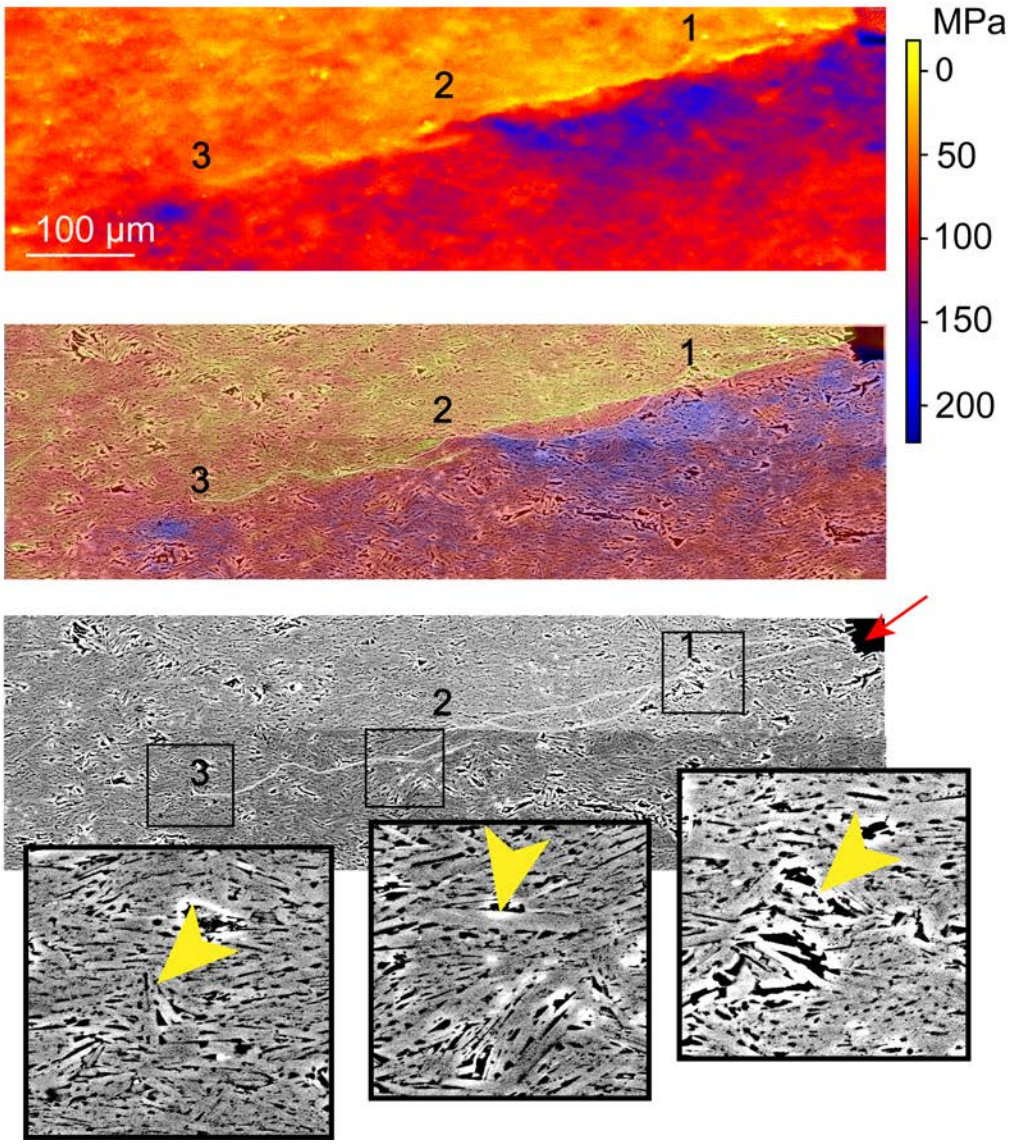

Figure 3. Crack path and stress field obtained by mapping the stress field (top) is overlaid with the SEM mosaic image of the same area (bottom). Microstructural defects labeled 1 to 3 are the same as in Fig. 2. Enlarged SEM images reveal that defects (yellow arrows) that cause toughening are either large alumina platelets (point 2) or bundles of highly misoriented alumina platelets (1 and 3). The color scale is modified from Fig. 2 to enhance contrast. The notch tip (red arrow) appears black in the upper right corner of the SEM image. White lines on SEM images highlight the main cracks identified from sharp contrasts in the stress map. © (2022) H. Saad et al. (10.6084/m9.figshare.20072111)

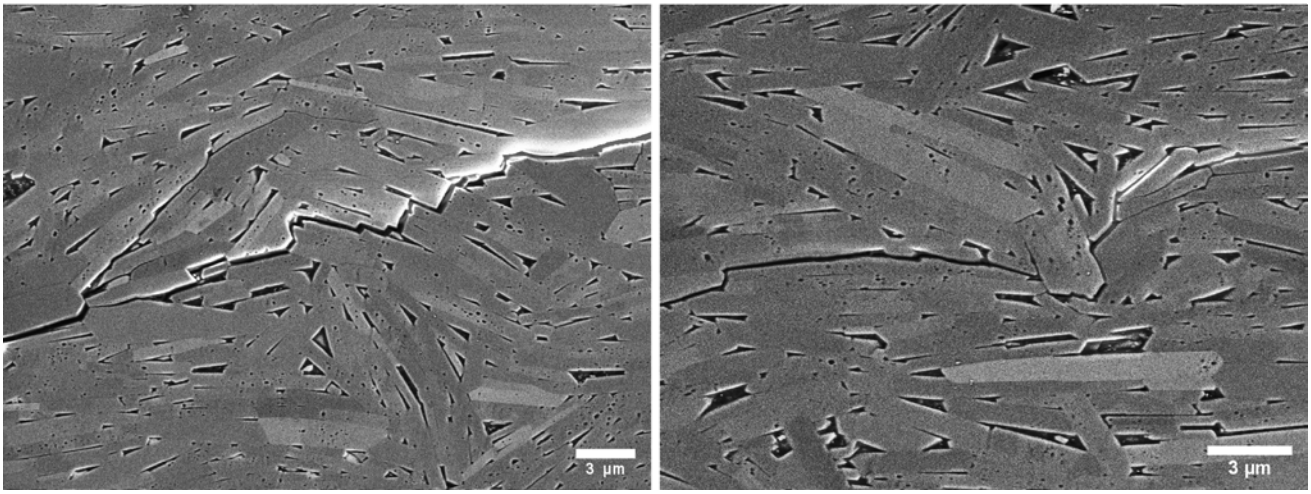

Figure 4. In situ SEM images of the open crack show crack branching (left) or deviation (right) around interlocking bundles of alumina platelets. These defects slow down crack propagation, and are associated with the mechanical asperities and crack pinning revealed by fluorescence imaging (Figs. 2 and 3). © (2022) H. Saad et al. (10.6084/m9.figshare.20072111)